

Experimental and numerical analysis of resistance spot welded joints on DP600 sheets

Z. Bézi, B. Baptiszta, S. Szávai

Research Fellow, Bay Zoltán Nonprofit Ltd. for Applied Research, Department of Structural Integrity

E-mail: zoltan.bezi@bayzoltan.hu

Keywords

Finite element analysis (FEA), spot welding (RSW, GTASW), advanced high strength steel, thermal-electric coupling, weld nugget, residual stress

1. Introduction

The development trends in the automotive industry show that the increase of fuel efficiency by weight reduction while maintaining and improving the safety of the passengers are crucial for the manufacturers. The economic recession and the rising oil prices forced the automotive manufacturers to favour conventional and advanced high strength steels against traditional mild steels. So it comes as no surprise that the share of advanced high strength steels in a modern automotive can be as high as 80% [1]. The most commonly used advanced high strength steels in the automotive industry are the so-called dual-phase or DP steels right now. The usage of dual-phase (DP) steel is favoured in strength dominant energy absorption parts and high strain parts thanks to the high ultimate tensile strength and good formability of said steels. These favourable characteristics are achieved by thermo-mechanical processing during which the formation of essentially two phases, ferrite and martensite take place.

As it was mentioned dual phase steels consist of ferrite matrix containing a hard martensitic second phase. Ferrite is soft and contributes to good formability, whilst martensite is hard and contributes to the strength of the material. The strength increases with a larger proportion of the hard martensitic phase [2].

Welding is the most commonly used joining process in the automotive industry so the investigation of the obtainable quality of welded joints produced by different welding processes on DP steels is relevant in the planning of future manufacturing processes.

The most dominant welding processes in the automotive industry, resistance spot welding (RSW) with single-pulse (SPC) and two-pulse current (TPC) spot welding are selected for the study.

In the present paper, a two-dimensional axisymmetric thermal-electrical-mechanical-metallurgical finite element (FE) model has been developed to investigate the distribution of temperature and nugget formation during RSW process of two DP 600 sheets. The results of finite element analyses were compared with the experimental measurements. The experimental procedures including sample fabrication and weld nugget size, residual stress and hardness measurements were followed by the modelling results.

2. Experimental procedure

The tests were carried out on DP 600 steel sheets with a thickness of 1 mm. Resistance spot welding (RSW) with both

single-pulse and two-pulse current spot welding were used to produce the welded joints. Resistance spot welding was carried out with copper alloyed (A2) spherical electrode with electrode face diameter of 5 mm as it is shown in Figure 1. The welding parameters were selected according to literature [2], [3] and preliminary welding tests. The results of these tests show that welding with the following parameters produce weld nuggets with a diameter of 5 mm in every case.

Two specimens were made for every welding process so residual stress analysis by X-ray Diffraction (XRD) can be performed on them. The analyses were performed according to EN 15305. Measurements were started at the centre of the spot weld and were repeated along the length of the specimens in 0.5 mm steps for 6 mm, so stress distribution can be determined in the weld, HAZ and base material as well.

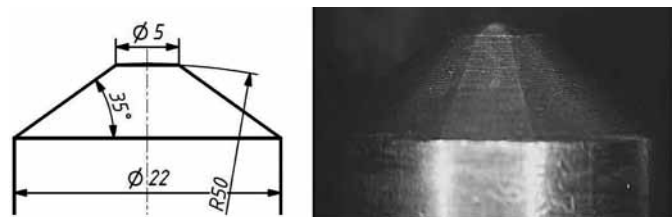


Figure 1. Electrode geometry.

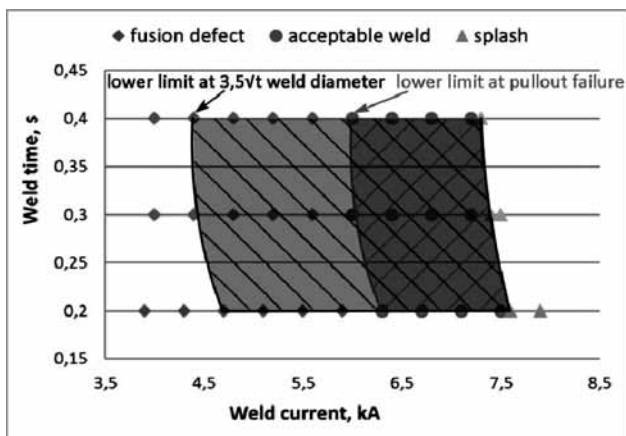
Determining the weldability lobe is crucial because it shows how flexible the welding process is for the given task. The larger the lobe is the more freedom it gives for the welding engineer and welding personnel concerning the selection of welding parameters.

The weldability lobe determinations were performed according to ISO 14327. The results are shown in Figure 2.

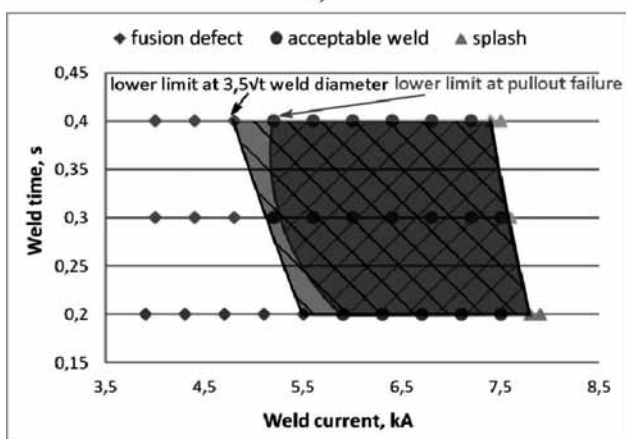
According to the standard the lower limit of the weldability lobe at constant electrode force should be at the welding conditions which result in a weld diameter equal to $3.5\sqrt{t}$ where t equal sheet thickness in mm [4]. However as it can be seen from the figures in case of DP 600 and mostly in case of SPC welding at $3.5\sqrt{t}$ weld diameter the typical failure mode is interfacial failure which should be avoided because it is associated with lower load bearing capacity and considerably less energy absorption capability [5].

The preferred failure mode is pullout failure which can be achieved if the lower limit of the weldability lobe is set at welding parameters which produce welded joints with failure load of 80-90% of the maximum failure load.

Comparing the weld lobes it can be stated that the weld lobe of RSW with TPC is wider than the weld lobe of RSW with SPC. According to the literature [7] the widening of the lobe is caused by the cooling time between the pulses.



a)



b)

Figure 2. Weldability lobes, a) RSW with SPC, b) RSW with TPC.

The load bearing capacity of a spot welded joint mainly depends on the weld nugget size so it is essential to inspect welded joints with approximately identical weld nugget size to be able to perform cross tension and peel testing. A weld diameter of 5 mm was selected for the tests. The experience from the production of the shear test specimens and preliminary welding trials complemented with macroscopic examinations were utilised to determine the welding parameters which result in appropriate weld nugget size. These welding parameters are shown in Table 1.

Table 1. Welding parameters of resistance spot welding.

Welding process	Squeeze time, [cycles]	Weld time, [cycles]	Cooling time [cycles]	Hold time, [cycles]	Weld current, [kA]	Electrode force, [kN]
RSW with SPC	30	15	-	20	6	2.75
RSW with TPC	30	7.5+7.5	20	20	7.2	2.75

Table 2. Test results.

Peel test results				Cross tension test results			
RSW with SPC		RSW with TPC		RSW with SPC		RSW with TPC	
F_{p11}	1.15 kN	F_{p21}	1.15 kN	F_{c11}	3.90 kN	F_{c21}	4.60 kN
F_{p12}	1.20 kN	F_{p22}	1.15 kN	F_{c12}	4.20 kN	F_{c22}	4.20 kN
F_{p13}	1.10 kN	F_{p23}	1.15 kN	F_{c13}	4.20 kN	F_{c23}	5.20 kN
Mean value	1.15 kN	Mean value	1.15 kN	Mean value	4.10 kN	Mean value	4.67 kN

Against the usual approach the cooling time was set higher than the welding time because the literature [7] suggests that in the case of resistance spot welding of DP steels there is a range in the cooling time between 15 and 30 cycles where local hardness spikes at the edge of the fusion zone can be avoided thus the preferable pullout failure mode can be achieved.

It is common practice in the industry to determine the weld nugget size from the post-tested peel test specimens. However from previous experience it can be stated that this method is not very accurate and gives only an approximate value for the weld diameter.

After the proper welding parameters were determined the cross tension and peel testing specimens were manufactured with given parameters in Table 1. The results of these tests are shown in Table 2.

Although Table 2 shows that only three specimens were tested so far-reaching conclusions cannot be made, the results can give guidance and show trends. While the peel tests yield similar values the cross tension test clearly shows that resistance spot welding with two-pulse current produces the best results.

3. Finite element modelling

For better understanding the reason of the differences between the test cases and further investigation of the proper welding parameters detailed finite element model has been built up as well.

FE modelling of the spot welding process can be difficult for most of the modelling tools including finite element based software, as RSW is governed by electrical-thermal, mechanical and metallurgical phenomena. To solve these complex problems, a FE based software MSC.Marc and Simufact.welding solvers were used in this study. It is difficult to simulate the RSW process because three different physical phenomena are interacting with each other. The model takes the following physical and metallurgical interactions into consideration in the simulations: interaction between the electro-kinetics and heat transfer via the Joule effect, heat transfer and phase transformations through latent heat and heat transfer, electro-kinetics, and mechanical behaviour via contact conditions [8].

The welding process starts with analysing the squeeze cycle in which electrode force is applied to the electrodes. The results of this mechanical analysis include initial deformations and contact area, which serve in electro-thermal analysis. In this

stage, the temperature distribution by Joule heating is calculated for an increment from the fully coupled electrical thermal FEA. In the electrically thermally coupled analysis the electrical and thermal boundary conditions are applied to the model in a house. Then the calculations of Joule heating at the sheet-sheet and electrode-sheet faying surfaces, as well as in the base material and electrode have to be performed. As a result, the temperature distributions are obtained in the first increment and sent to the mechanical analysis as a nodal thermal load.

Contact pressure and deformations are the results of mechanical analysis that obtains a new contact condition. So, the mechanical results are transferred to the electro-thermal analysis to update contact conditions for the next increment analysis. This loop continues until the welding time is finished [15]. This applies for both single-pulse and two-pulse current welding as well.

In the FEA of RSW, joint geometry is represented by a two-dimensional axisymmetric model. The associated element mesh is shown in Figure 3. Four-node axisymmetric elements were used to model the electrode and the steel sheets. The finite element mesh contains 2350 elements and 2597 nodes. The mesh is graded from fine to coarse, according to the expected reduction in temperature gradient on moving away from the heat source. Solid elements were employed to simulate the thermo-elastic-plastic behaviour of the sheets and electrodes. Contacts were employed to simulate the contact areas. There were three contact areas in the model, two represent the electrode-sheet interface and another one represents the faying surface. They were all assumed to be contact between two deformable surfaces, and these surfaces were allowed to undergo small sliding.

Thermal-electric and mechanical boundary conditions were applied to the FE model. Heat transfer to the surrounding air, using convection and 20 W/m²K convective heat transfer coefficient was used. At the far end of the steel sheet and water temperature inside the copper electrode were assumed to be at ambient temperature of 20°C. At the top electrode, the electrical current was applied uniformly to the top of the electrode.

In the analysis of mechanical deformation during welding, the thermal load was applied to each nodal point, while the symmetry

line of the model was allowed to extend only along the vertical axis, with no lateral displacement. The welding parameters are the same as in the case of the physical specimens (Table 1).

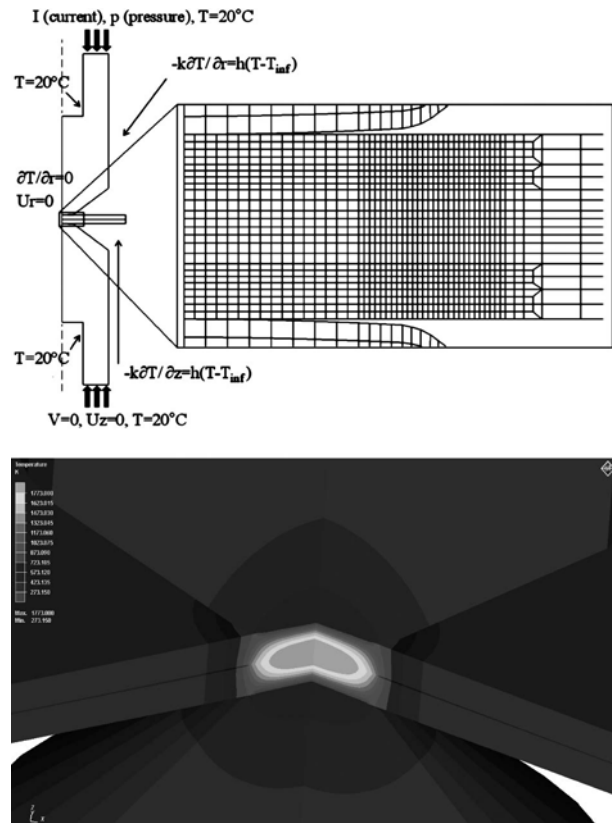


Figure 3. FE model.

In order to predict accurate results, all of the relevant mechanical, thermal and electrical properties of the steel sheets and copper electrodes must be known. Since electrical and physical properties vary with temperature and are not readily available, many of these values are estimated from literature and assumed to be homogeneous [9] [10]. Contact resistivity of the sheet-to-sheet and electrode-to-sheet interfaces were also assumed to vary with temperature. Some essential thermo-

Table 3. Thermal and electrical properties [8].

Temp. [°C]	Electrical resistivity DP600 [Ωm•10 ⁻⁷]	E. contact conductance sheet/sheet [1/Ωm•10 ⁹]	E. contact conductance electrode/sheet [1/Ωm•10 ⁹]	T. contact conductance sheet/sheet [W/m ² °C]	T. contact conductance electrode/sheet [W/m °C]	Thermal Conductivity DP600 [W/m°C]
20	2.041	0.203	1.075	250000	20000	43.5
100	2.703	0.298	2.174	-	-	43
200	3.332	0.401	3.334	-	-	42
300	4.348	0.505	4.348	-	-	38
500	6.452	0.714	6.668	-	-	29
700	9.524	0.909	8.621	-	-	17
1000	11.90	1.222	12.05	-	-	11.5
1300	12.35	1.538	16.67	-	-	19
1600	15.38	1.852	18.52	-	-	28
2000	15.63	3.025	26.13	4570000	4000000	33

electrical properties parameters of steels are used in the model for DP 600 are listed in Table 3 [8].

During the analysis, a full Newton–Raphson iterative solution technique with direct sparse matrix solver is employed for obtaining a solution. During the thermal analysis, the temperature and the temperature-dependent material properties change very rapidly. Thus it is believed that, a full Newton–Raphson technique using modified material properties gives more accurate results [15].

4. Mechanical properties

In order to capture the correct microstructure evolution a number of material properties are required for present simulations. The elastic behaviour is modelled using the isotropic Hooke’s rule with temperature-dependent Young’s modulus. The thermal strain is considered using thermal expansion coefficient. The yield criterion is the Von Mises yield surface. In the model, the strain hardening is taken into account using the isotropic Hooke’s law. The thermo-metallurgy material properties of DP 600 steel were generated with JMatPro software based on its chemical composition.

Transformation data was calculated using Simufact.premap interface with 10 μm grain size starting at 1050°C. The flow curves were calculated with 30 μm grain size starting at 1300°C.

The mixture of the initial microstructure elements in the FE model has to be defined. In the present simulation 65% ferrite and 35% martensite initial fractions were used. Strain hardening at room temperature is shown in Figure 4.

Cu-Cr-Zr alloy, which has high thermal conductivity performance, is selected for electrodes. Non-linear time dependency of thermal and electrical material properties as well as convection coefficient rate for water, air and gas flow are all obtained from literature and paper [9].

5. Results and discussion

RSW models were validated with available experimental results. A simulation model has been developed and extensive numerical calculations were carried out to find out the spot diameter and residual stress distribution of resistance spot welded DP600 joints.

The answers of the simulation include the nugget size, the radius of the heat affected zone (HAZ) and the volume of

the molten zone. The molten zone is the region of the sheets where the actual weld is formed, while the heat affected zone is the adjacent region where heat may cause solid state phase transformation, but melting does not occur. An additional capability of the model is the ability to predict the volume fraction of various microstructure elements. The volume fraction of austenite, ferrite and martensite can be quantified and serve as an additional response that can be used to validate this model with experiments and to predict microstructure element volume fractions under new processing conditions [8], [11], [12].

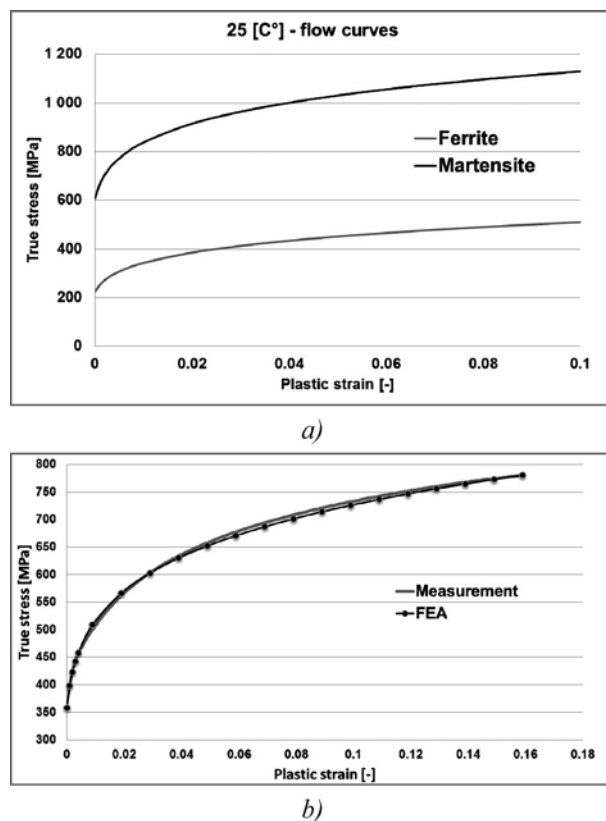


Figure 4. Strain hardening, a) Strain hardening at room temperature, b) Strain hardening comparison.

Figure 5 is the optical micrograph of specimen SPC RSW, and it shows that the typical microstructure of spot weld including crystallized morphology in fusion zone. The figure compare temperature contours with SPC RSW experimental

Table 4. Thermo-mechanical properties of DP 600.

Temp. [°C]	Modulus of elasticity (Austenite) [GPa]	Modulus of elasticity (F./M./B./P.) [GPa]	Specific heat capacity (Austenite) [kJ/kg°C]	Specific heat capacity (F./M./B./P.) [kJ/kg°C]	Thermal expansion (Austenite) [1/°C•10 ⁻⁵]	Thermal expansion (F./M./B./P.) [1/°C•10 ⁻⁵]
20	197	208	0.453	0.447	2.53	1.289
100	190	205	0.475	0.479	-	-
200	181	199	0.497	0.519	-	-
400	163	181	0.532	0.623	-	-
500	154	169	0.549	0.697	-	-
800	125	126	0.595	0.799	-	-
950	110	103	0.611	0.714	-	-
1050	100	87	0.639	0.701	2.566	1.663

micrographs, the colours represents the heat affected zone, where the material is partially transformed into austenite. In the HAZ near base metal there is a fine-grained region, while in the HAZ near the fusion boundary there is a coarse grained region. The size of fusion zone, HAZ is again in good agreement with the experimental observations.

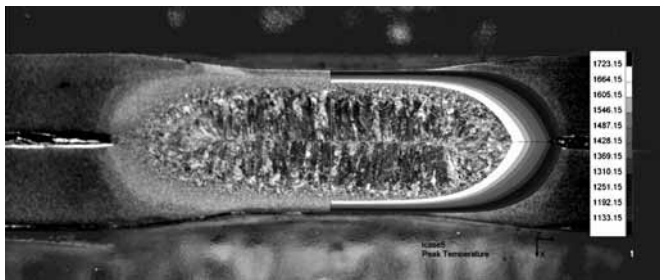
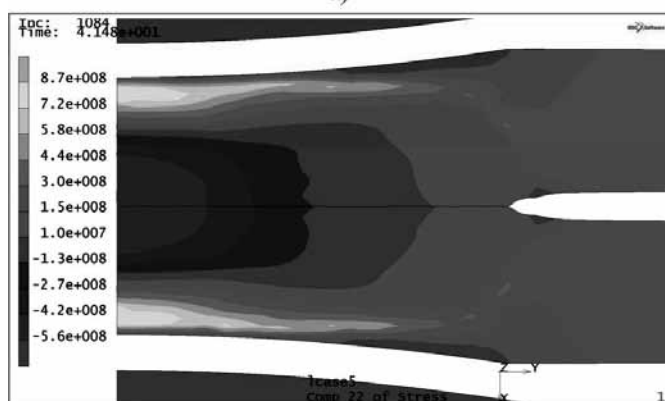


Figure 5. Comparison of simulation results with experimental test in case of SPC RSW.

The residual stresses have different values on the surface of the spot welded specimen. The stress and strain field in the specimen during the RSW process is very complex due to the combination of temperature and electrode force. In the final stage of the welding processes, the nugget and its neighbouring



a)



b)

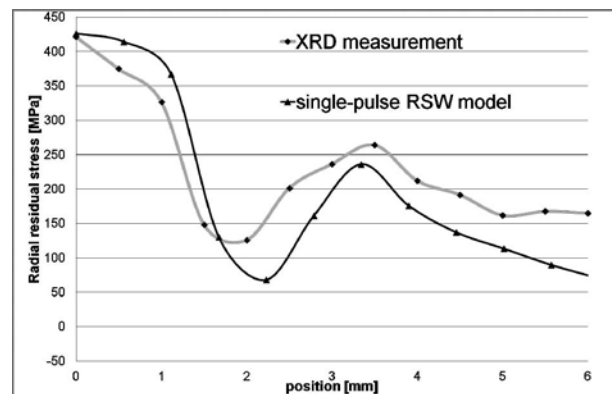
Figure 6 RSW measurement and result of the simulation, a) XRD measurement, b) Radial residual stress after RSW [Pa].

zones tend to expand and contract and these phenomena induce an undesirable effect on remaining parts of the specimen. The internal stresses due to heterogeneous deformations are known as residual stresses. In resistance spot welding process, there is another factor that affects the residual stresses' state. This factor is the electrode force that develops compressive stress in the

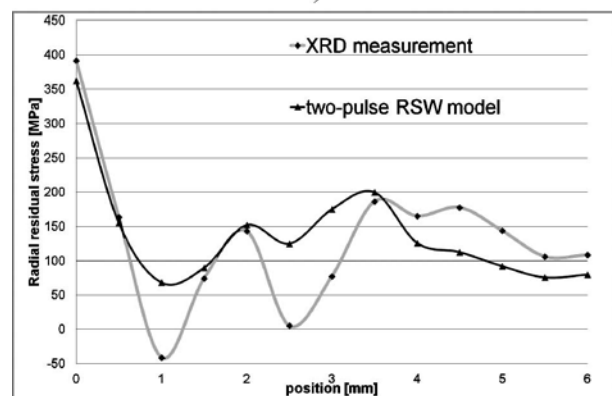
weld nugget [10]. The position of residual stress measurements are shown in Figure 6a.

Radial residual stresses are studied employing XRD experiments and FEM simulation. In this process due to axial symmetry of the system, directions of 2D principal stresses are the same as directions of radial and circumferential. Distribution of radial residual stresses for sample SPC RSW is shown in Figure 6b. Residual stresses have also been measured along the length of the specimens in 0.5 mm steps for 6 mm in all samples. The results of diffraction for the sample RSW is shown in Figure 7. Although the distribution shape of the radial residual stress predicted by the numerical model is similar to the measured values by the experiment weld nugget zone, the magnitudes predicted by the numerical model are larger than the measured data and lower in other region; however the simulated results have a good agreement with the measured data.

Residual circumferential stresses in the model are tensile in weld nugget while they are compressive in the neighbouring regions of the nugget. It is observed that the largest residual stress exists at the central region of the weld nugget and it is decreasing towards the outer sides [13][14].



a)



b)

Figure 7. Comparison of calculated and measured residual stress data, a) Radial residual stress after SPC RSW, b) Radial residual stress after TPC RSW .

The focus is on the residual stress around the nugget edge because the tensile residual stress around it contributes most in increasing the maximum stress of spot welded specimen. Especially the normal residual stress in the radial direction affects the maximum stress status in any loading type. Therefore, the following results are restricted to the radial direction of the normal stress around the nugget edge.

Due to the dual microstructure of DP steels the correct austenitic/martensitic ratio is hard to measure and can only be estimated, therefore the residual stress caused by the volumetric change of martensitic transformation slightly differs in the simulation and the measurement. In the case of RSW with two-pulse current the welding conditions at the first weld time have little effect on the residual stress. But at the second weld time, the magnitudes of weld current and weld time produce a considerable effect on the residual stress. As the second weld current increases, the residual stress becomes smaller. These phenomena are due to the difference of contribution to the heating energy. The increase of both weld current and weld time decreases the residual stress because the increase of heat input makes the temperature gradient gentle along the z-direction just after welding [9].

7. Acknowledgement

The research work presented in this paper is supported by the TÁMOP-4.2.2.A-11/1/KONV-2012-0029 project. The project is co-financed by the European Union and the European Social Fund.

References

- [1]. World Steel Association: Advanced High Strength Steel (AHSS) Application Guidelines, Version 4.1., June, 2009, p.: 1-16, www.wordautosteel.org
- [2]. T. Nilsson, Welding of AHSS/UHSS Steel – A guide for the automotive industry, 332en, 2012, p.:21-22.
- [3]. T. Nilsson et al., Sheet steel joining handbook, SSAB Tunplåt AB, 2004
- [4]. ISO 14327: “Resistance welding. Procedures for determining the weldability lobe for resistance spot, projection and seam welding”
- [5]. Y. J. Chao: Failure mode of spot welds: interfacial versus pullout, Science and Technology of Welding and Joining, Vol. 8, No. 2, 2003

[6]. L. Prém: A technológiai paraméterek kísérleti úton történő optimalizálása a DP acélok ponthegeztése során, Tavaszi Szél Konferencia, Debrecen, 2014

[7]. L. Prém: The influence of technology on the structure of spot welded joints of high-strength DP steels, 27th Welding Conference, Budapest, 2014 (under publication)

[8]. M. Eshraghi, M.A. Tschopp, M.A. Zaem, S.D. Felicelli, Effect of resistance spot welding parameters on weld pool properties in a DP600 dual-phase steel: A parametric study using thermomechanically-coupled finite element analysis, Materials and Design (2014) Vol. 56, pp. 387-397.

[9]. I. Ranjbar Nodeh, S. Serajzadeh, A.H. Kokabi, Simulation of welding residual stresses in resistance spot welding, FE modeling and X-ray verification, Journal of materials processing technology (2008), Vol. 205, pp. 60–69.

[10]. Zhigang Hou, Ill-Soo Kimb, Yuanxun Wang, Chunzhi Li, Chuanyao Chen, Finite element analysis for the mechanical features of resistance spot welding process, Journal of Materials Processing Technology 185 (2007), pp. 160–165.

[11]. Khan MI, Kuntz ML, Su P, Gerlich A, North T, Zhou Y. Resistance and friction stir spot welding of DP600: a comparative study. Sci Technol Weld Joining (2007), Vol. 12, pp. 175-82.

[12]. Anastassiou, M., Babit, M., Lebrun, J.L., Residual stress and microstructure distribution in spot welded steel sheets: relation with fatigue behavior. Materials Science and Engineering. (1990) A 125, 141–156.

[13]. B-W. Cha and S-J. Na. A Study on the Relationship Between Welding Conditions and Residual Stress of Resistance Spot Welded 304-Type Stainless Steels, Journal of Manufacturing Systems (2003) Vol. 22/No. 3

[14]. Hessamoddin Moshayedi, Iradj Sattari-Far, Numerical and experimental study of nugget size growth in resistance spot welding of austenitic stainless steels, Journal of Materials Processing Technology (2012) Vol. 212, pp. 347–354.

[15]. MSC.Marc 2012. Theory and User Information

